Shapes of rolling liquid drops

By PASCALE AUSSILLOUS[1,2] AND DAVID QUÉRÉ[2]

[1]Institute of Theoretical Geophysics, Department of Applied Mathematics and Theoretical Physics, University of Cambridge, CMS, Wilberforce road, Cambridge CB3 0WA, UK

[2]Laboratoire de Physique de la Matière Condensée, UMR 7125 du CNRS, Collège de France, 75231 Paris Cedex 05, France

We describe here liquid drops in rotation, and first classify the different shapes possible. Then, we study the behaviour of liquid marbles, which are droplets coated with hydrophobic grains, running down inclines. Because these marbles roll as they move, this device allows us to achieve revolving drops. We report the different forms generated during the descent, and quantify their size by way of scaling arguments. We finally focus on the transformations which may occur between different drop shapes.

1. Introduction

Physicists and mathematicians have been interested in the shapes of rotating globules for more than two centuries, in particular because of the connection between this issue and the shape of celestial bodies. Most of the studies remained theoretical and focused on the ideal case of isolated revolving drops. When such a body is put in rotation, the centrifugal force deforms it, while surface tension tends to restore a spherical form. It is thus not surprising to find, at the beginning of this research, Laplace (1843), who both first described capillarity and was a pioneer in celestial mechanics. Then came Plateau, one of the few experimentalists working in this field, who used as a model system an oil drop immersed in a mixture of water and alcohol of the same density. The oil drop is spherical at rest, and can be put into a state of rotation by passing a solid axis through it (Plateau 1843). This experiment remains difficult to interpret however, because of the action of the outer liquid which cannot be neglected; in particular, matching the densities of the two fluids should make negligible the action of centrifugal force. In 1885, Poincaré did the first extensive study on the equilibrium shapes of rotating drops, and showed that two very different classes of solution may be generated: on the one hand, axisymmetric shapes, which include disks or even tori (also mentioned by Ross 1968); on the other hand, asymmetric shapes, characterized by two lobes (Poincaré 1885).

Lord Rayleigh solved analytically the equations of the motion in different simple cases, which allowed him to explain some of Plateau's observations (Rayleigh 1914). In a famous analogy, Bohr & Wheeler (1939) proposed modelling nuclear fission as the rupture of a rotating liquid drop: considering the nucleus as a charged liquid drop, they treated the fission as a division of the liquid sphere, with surface tension playing the role of nuclear forces. A review devoted to a unified discussion on configurations of atomic nuclei, revolving astronomical bodies and rotating drops can be found in Cohen, Plasil & Swiatecki (1974). Chandrasekhar (1965) described theoretically the
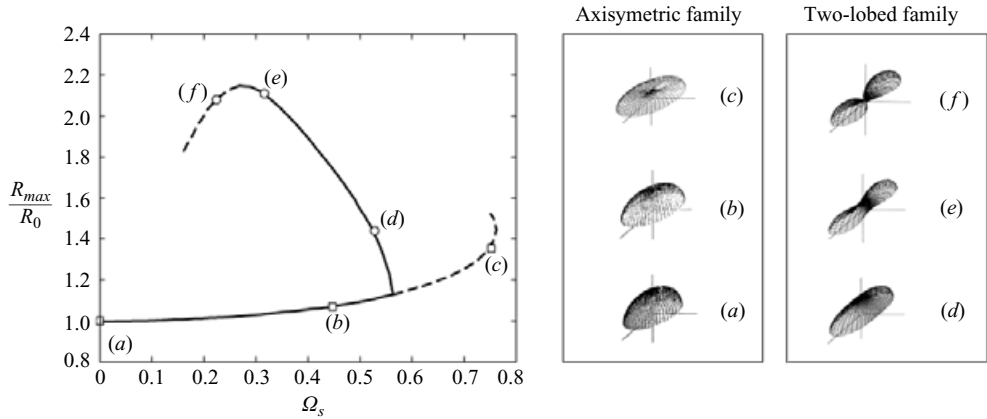
FIGURE 1. Phase diagram of axisymmetric (*a*, *b*, *c*) and two-lobed (*d*, *e*, *f*) isolated drops in rotation (Brown & Scriven 1980*a*). The maximum size of the centrifuged drop is normalized by its initial radius and plotted as a function of the angular speed of rotation Ω_s made dimensionless as defined in equation (1). The full lines indicate stable shapes. Six examples of shapes computed by Brown & Scriven are also displayed.

configuration of rotating liquid drops and was the first to consider the question of the stability of the different shapes. He noted the similarity between his solutions and the appearance of various planets, including Saturn's rings (yet stressed that this was a coincidence). This rapid overview ends with the comprehensive work by Brown & Scriven, who solved numerically the equations of motion and discussed very precisely the stability of the different possible shapes (Brown & Scriven 1980*a*, *b*). Their main results are summarized in figure 1, where the maximum size R_{max} of the centrifuged drop normalized by its initial radius R_0 is plotted as a function of the angular speed of rotation ω. Because of the opposing roles of centrifugal and capillary forces, it is logical to construct a dimensionless number which compares these actions. Following the notation introduced by Brown & Scriven, we define the *rotation number* Ω_s by

$$\Omega_s = \sqrt{\frac{\rho \omega^2 R_0^3}{8\gamma}}. \tag{1}$$

where ρ is the liquid density, and γ its surface tension.

Brown & Scriven found numerically four families of solutions: axisymmetric, two-lobed, three-lobed and four-lobed shapes. We show the axisymmetric and the two-lobed families in figure 1, where the normalized maximum size of the drop is plotted as a function of the rotation number Ω_s. The lower line (*a*, *b*, *c*) corresponds to the axisymmetric family. On increasing the angular speed, the drop evolves from a sphere to an ellipsoid flattened at the poles, then to a disk and eventually to biconcave shapes (a disk-like shape hollowed at the centre). Above a maximum angular speed ($\Omega_s = 0.754$), no further axisymmetric shapes can be calculated: capillary forces cannot counterbalance centrifugal forces. Nevertheless, the axisymmetric family does not end at $\Omega_s = 0.754$, but continues with lower angular speeds. This branch ends when the thickness at the centre of the drop becomes zero. The upper line (*d*, *e*, *f*) in figure 1 corresponds to the two-lobed shapes. Brown & Scriven predicted that such isolated

(i.e. with a constant angular momentum) drops are more stable than axisymmetric ones, in the regime of 'large' deformations. This defines in figure 1 stable branches (shown with a solid line), and an unstable one (dots). At the intersection point , they found $\Omega_s \approx 0.56$; at this point, the drop is an ellipsoid.

From an experimental point of view, the main difficulties are to isolate a drop from other external forces (gravity, wetting on a substrate, etc.), and to make such a drop rotate. Nevertheless, some techniques have been proposed for making it, such as the use of a jet of air, or acoustic waves in microgravity (Wang *et al.* 1986; 1994; Lee *et al.* 1998). These experiments allowed to the deformations to be described in the regime of moderate Ω_s, and confirmed the existence of a bifurcation to two-lobed shapes. Here we propose using *liquid marbles*, which spontaneously rotate as they move on solid substrates. These are liquid drops coated with a hydrophobic powder (Aussillous & Quéré 2001). The powder stays at the surface of the drop and isolates it from the solid on which it is deposited: we then observe a purely non-wetting behaviour, whatever the nature of the substrate. If these marbles are small (i.e. of radius smaller than the capillary length $\kappa^{-1} = \sqrt{\gamma/\rho g}$ (where γ is surface tension and ρ density), 2.5 mm in our experiments), they are nearly perfect spheres. Larger ones are flattened by the action of gravity and form puddles. The coating powder we used is natural lycopodium, namely the spores of a moss, of typical size 30 μm. The grains are treated with a fluoro-decyl-trichlorosilane, which enhances their natural hydrophobicity. For liquids, we used mixtures of water and glycerol, which provide solutions with a wide range of viscosity η (between 100 and 1200 mPa s) with a nearly constant surface tension γ (between 72 mN m^{-1} and 63 mN m^{-1}) and density ρ (between 1000 kg m^{-3} and 1200 kg m^{-3}).

If deposited on an incline, these marbles run down, and the descent velocity can be adjusted by tuning the tilting angle α. If α is small (typically smaller than 10°), the drop keeps a quasi-static shape as it moves. Using the surface grains as tracers, it is observed to fully rotate, as predicted by Mahadevan & Pomeau (1999) who showed that such a solid-like motion is favoured at small Reynolds numbers. For a millimetric drop of glycerol ($\eta \approx 1000$ mPa s), the Reynolds number $Re = \rho V R_0/\eta$ (where V is drop velocity) remains smaller than unity if the velocity is below 1 m s^{-1} – a condition which is not very restrictive, since this speed is comparable with the terminal velocity of a drop falling in air. Yet the centrifugal force associated with the drop rotation can be quite large (compared with the capillary force). Supposing a rigid-body rotation ($V = \omega R_0$), a Weber number comparing these two forces can be introduced:

$$We = \frac{\rho V^2 R_0}{\gamma}. \tag{2}$$

This number is very similar to Ω_s (equation (1)). A condition of small Weber number implies velocities typically smaller than 25 cm s^{-1}, which can be easily exceeded by our liquid marbles on sharply inclined plates. Hence we expect significant deformations using this simple system, as confirmed in figure 2 which shows glycerol marbles running down plates inclined at an angle of 35°.

We observe 'peanut', disk and toroidal (wheel) shapes (Aussillous & Quéré 2001). The latter is reminiscent of a doughnut, but a very thin film remains at the centre as suggested by the reflection of the light in figure 2(*c*). We first describe this new shape, and discuss how it can be integrated into the phase diagram (figure 1) of Brown & Scriven. Then, we summarize the classification, using scaling arguments. We
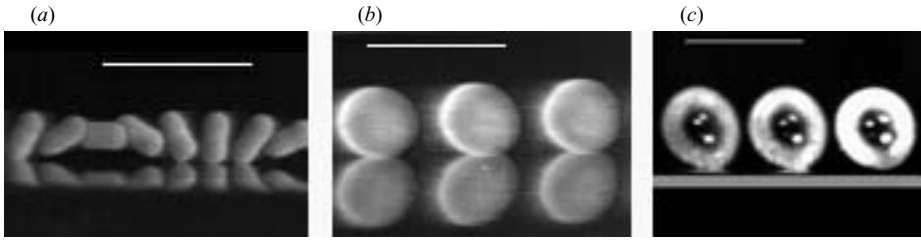
FIGURE 2. Liquid marbles (made of glycerol, and coated with lycopodium grains) rolling down a plate inclined by 35°. The initial radius R_0 is (a) 1, (b) 1.9 and (c) 1.9 mm, and the speed about $1.2\,\mathrm{m\,s}^{-1}$. The time intervals between the snapshots in (a)–(c) are respectively 1.1, 1.5 and 3 ms, and the bar indicates 1 cm. We observe either peanut, disk or wheel shapes.
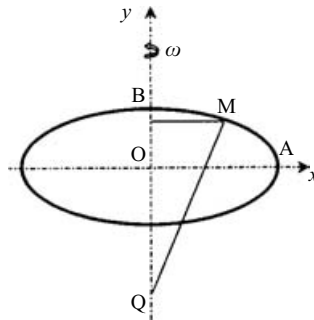

FIGURE 3. Sketch of an axisymmetric rotating liquid drop.

compare our experimental results with these predictions, and conclude by studying two examples of transformation between different drop shapes.

2. Toroidal drops

2.1. *Axisymmetric rotating drops*

We start from the Rayleigh equations describing axisymmetric revolving drops (Rayleigh 1914). The shape of the drop results from an equilibrium between the capillary and the centrifugal forces. We assume the motion to be a solid rotation at a constant angular speed ω (figure 3).

In the rotating reference frame, the drop is at rest and we can calculate the pressure at a point M on the surface by expressing the balance of forces:

$$P = \frac{\rho\omega^2 x^2}{2} + P_0, \tag{3}$$

where P_0 is the pressure on the axis of rotation, and x the distance to this axis. Moreover, the Laplace law can be written:

$$P = P_{ext} + \gamma C, \tag{4}$$

with P_{ext} the atmospheric pressure (set for convenience equal to 0), and C the interface curvature. For a surface of revolution, C can be expressed using the curvilinear

abscissa s along a meridian:

$$C = \frac{\mathrm{d}^2 y/\mathrm{d}s^2}{\mathrm{d}x/\mathrm{d}s} + \frac{1}{x}\frac{\mathrm{d}y}{\mathrm{d}s}. \tag{5}$$

Combining the above equations and integrating yields

$$x\frac{\mathrm{d}y}{\mathrm{d}s} = \frac{\rho\omega^2 x^4}{8\gamma} + \frac{P_0 x^2}{2\gamma} + K, \tag{6}$$

where K is a constant of integration. In addition, we have

$$\frac{\mathrm{d}y}{\mathrm{d}x} = \frac{\mathrm{d}y/\mathrm{d}s}{\sqrt{1 - (\mathrm{d}y/\mathrm{d}s)^2}} \tag{7}$$

where $\mathrm{d}y/\mathrm{d}s$ is given by equation (6). It is then possible to obtain numerically the shapes of axisymmetric rotating drops by introducing appropriate boundary conditions.

2.2. *Numerical shape of the wheel*

For a wheel, there is no liquid on the axis of rotation. However, we observe experimentally that a thin film persists at the centre of the ring. So, we assume that we can find R_1 and R_{max} ($R_1 < R_{max}$) on the axis (i.e. for $y = 0$), with a vertical tangent ($\mathrm{d}y/\mathrm{d}s = 1$) for $x = R_{max}$ and a horizontal one ($\mathrm{d}y/\mathrm{d}s = 0$) for $x = R_1$. Equation (6) becomes:

$$x\frac{\mathrm{d}y}{\mathrm{d}s} = \frac{\rho\omega^2}{8\gamma}\left(x^2 - R_1^2\right)\left(x^2 - R_{max}^2\right) + R_{max}\frac{x^2 - R_1^2}{R_{max}^2 - R_1^2}. \tag{8}$$

There are three unknowns in equation (8), namely the radial lower and upper radii (R_1 and R_{max}) of the wheel and the angular velocity. However, all the shapes should be determined by only two parameters, typically the volume and the angular velocity. As there is no obvious relationship between the three unknowns, it means that once two unknowns are fixed, the third one has to be determined *a posteriori* to satisfy the boundary conditions. The conditions on the tangents are included in equation (8), so that the only remaining boundary condition is $y(x = R_1) = y(x = R_{max}) = 0$.

One of the fixed parameters is naturally the angular velocity. The other cannot simply be the volume since it does not appear directly in equation (8) (yet it is easily deduced once the shape obtained). We chose to fix R_{max} and to use R_1 as an adjustable parameter. To calculate the shape for a given couple (R_{max}, ω), we integrate numerically equation (7) using equation (8), with a constant increment $\mathrm{d}x$. We start from the point $x = R_{max}$, $y = 0$ to avoid beginning the integration with a horizontal tangent. When the shape is obtained, R_1 is varied to obtain the only conformation which satisfies the boundary condition $y(x = R_1) = 0$. The volume is finally calculated numerically, from which we deduce the initial radius R_0.

We worked with a constant maximal length R_{max} and increased the angular speed of rotation gradually. The different results are displayed in figure 4, where we show only one fourth of the profile – the whole shape can easily be deduced from symmetries relative to both axes.

All our numerical results are collected in figure 5 and included in Brown & Scriven's phase diagram, where the quantity R_{max}/R_0 is plotted as function of the normalized angular speed $\Omega_s = \sqrt{\rho\omega^2 R_0^3/8\gamma}$. The wheel family (represented with squares) is found
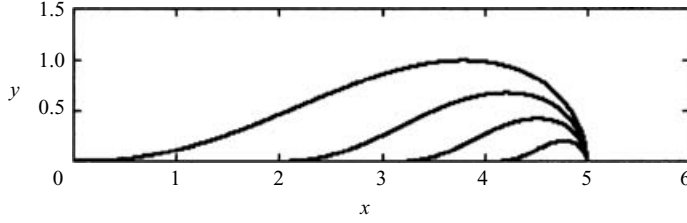
FIGURE 4. Numerical wheel shape of liquid drops in rotation for $\Omega_s = 0.705; 0.666; 0.644; 0.627$ (from top to bottom).
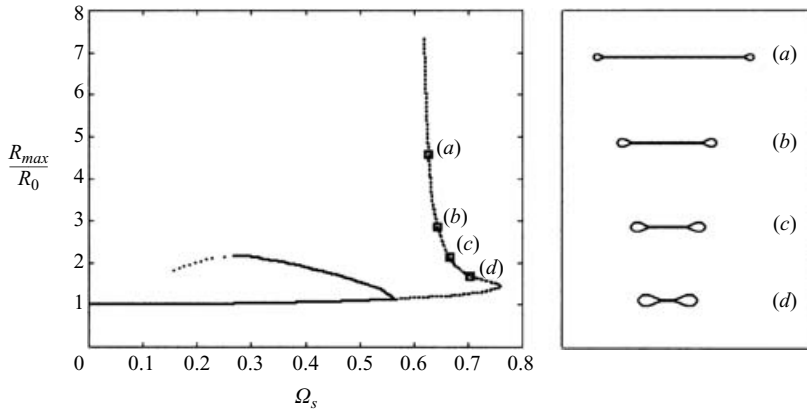

FIGURE 5. Maximum size of a centrifuged drop (scaled by its initial radius), as a function of the normalized angular speed of rotation Ω_s (defined in equation (1)). The branch with the squares represents the wheel family, which is found to match the axisymmetric family calculated by Brown & Scriven (figure 1). Other stable branches are indicated for interest, and side views of the numerical shapes corresponding to points (a), (b), (c) and (d) are displayed on the right.

to add a branch (a, b, c, d) in figure 5 in the continuity of the axisymmetric shapes (to which it belongs) calculated by Brown & Scriven.

2.3. Simple shapes

Revolving drops can be quite complicated geometrically, but some shapes (such as the disk or the torus, for example) appear to be particularly simple, and thus we were tempted to complement the numerical calculations by simple analytical or scaling arguments. We start with axisymmetric objects, and distinguish four well-defined objects (ellipsoids, disks, biconcave shapes and wheels), and represent them in figure 6. Each shape is calculated numerically, for a given value of Ω_s.

For small rotational speeds, the drop is an ellipsoid of large and small axes R_{max} and h (figure 6a). Rayleigh (1914) showed that expanding the equations of motion for $\Omega_s < 0.3$ yields as an analytical expression for R_{max}:

$$\Omega_s^2 = (R_0/R_{max})^3(1 - (R_0/R_{max})^3). \tag{9a}$$

In the same limit, we find for the small axis $h = R_{max} (1 - \Omega_s^2(R_{max}/R_0)^3)$. We shall refer to this shape in our summary figure 8 as 'ellipsoid 1'. For larger velocities ($0.3 < \Omega_s < 0.6$), higher-order expansions give an expression, that we call
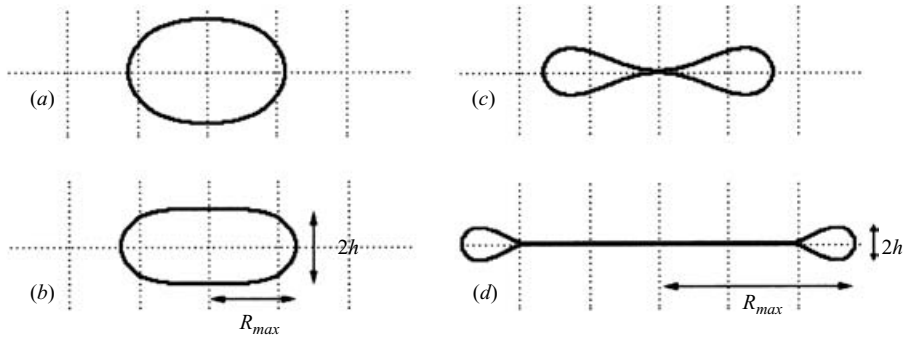
FIGURE 6. Numerical shapes of liquid drops in rotation around the vertical axis: (*a*) ellipsoid ($\Omega_s = 0.56$), (*b*) disk ($\Omega_s = 0.707$), (*c*) biconcave shape ($\Omega_s = 0.71$) and (*d*) wheel ($\Omega_s = 0.644$); (*d*) corresponds to the third shape in figure 4. We denote R_{max} and h as the maximum length and thickness of the centrifuged drop.

Shape	Disk	Pinched disk	Biconcave	Wheel
Figure	Figure 6(*b*)		Figure 6(*c*)	Figure 6(*d*)
Volume conservation	$R_{max}^2 h \sim R_0^3$	$R_{max} h^2 \sim R_0^3$	$R_{max} h^2 \sim R_0^3$	$R_{max} h^2 \sim R_0^3$
Gradient of pressure	γ/h^2	γ/h^2	$\gamma/(hR_{max})$	γ/h^2
Scaling law	$R_{max} \sim R_0 \Omega_s^{2/3}$	$\Omega_s \sim$ constant	$R_{max} \sim R_0 \Omega_s^{-4/3}$	$\Omega_s \sim$ constant
Equation	(10)	(11)	(12)	(13)

TABLE 1. Characteristics of the different axisymmetric shapes.

'ellipsoid 2':

$$\Omega_s^2 = \tfrac{1}{2}(R_0/R_{max})^3(1 - \sqrt{4(R_0/R_{max})^3 - 1}) \tag{9b}$$

and the small axis becomes $h = R_{max}(1 - \Omega_s^2(R_{max}/R_0)^3) + \Omega_s^4(R_{max}/R_0)^6)$.

For the other stationary shapes, there is a balance between the centrifugal force and the gradient of the Laplace pressure, with a constraint of constant volume. Thanks to the simulations, we know that some of these shapes are very close to simple objects (such as disk, wheel, etc.), allowing us to propose approximate expressions for the volume conservation and the capillary force, and thus estimates of the drop size. In each case, the centrifugal force (per unit volume) on an object of largest length R_{max} scales as $\rho\omega^2 R_{max}$. We denote as h the thickness of the drop, as defined in figures 6(*b*) and 6(*d*).

For the disk, for example, the Laplace pressure at the drop edge is $P = P_0 + \gamma/h$ (assuming $h \ll R_{max}$). The radial gradient of this quantity is $\nabla P \sim \gamma/h^2$. It tends to restore the spherical shape, and is balanced by the centrifugal force. Expressing the volume conservation $R_{max}^2 h \sim R_0^3$, we obtain

$$R_{max} \sim R_0 \Omega_s^{2/3}. \tag{10}$$

Similar arguments can be made for the different simple axisymmetric shapes, and we collect in table 1 the expressions for the volume conservation and the Laplace pressure gradient in each case. Balancing the capillary force with the centrifugal one, we obtain the size of the corresponding shape, which is also displayed in table 1.
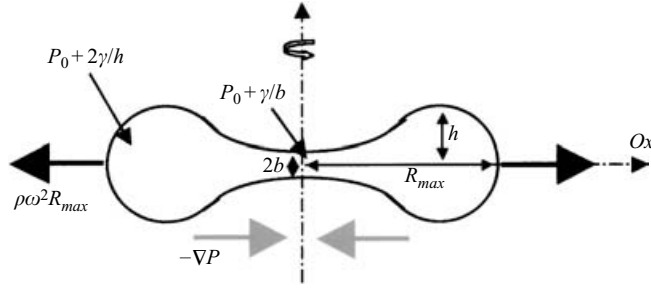
FIGURE 7. Forces acting on a two-lobed rotating drop.

The corresponding scaling laws for the pinched disk, the biconcave shape and the wheel are, respectively,

$$\Omega_s \sim \text{constant}, \tag{11}$$

$$R_{max} \sim R_0 \Omega_s^{-4/3}, \tag{12}$$

$$\Omega_s \sim \text{constant}. \tag{13}$$

Thus the wheel shape (equation (13)) should imply a vertical line in figure 5, as observed asymptotically. We can even find the value of the constant. The conservation of volume is written $2\pi^2 h^2 R_{max} = 4\pi R_0^3/3$, and the Laplace pressure γ/h (h being here the radius of the cylinder making the wheel), which yields a gradient of pressure close to $\gamma/2h^2$. Using equation (1), we thus deduce $\Omega_s \approx \sqrt{6\pi}/8 \approx 0.54$, close to the value deduced numerically (deduce $\Omega_s \approx 0.62$). Note that this regime is analogous to a rotating spring (of mass M and stiffness k) in the regime of large deformation. Then, the force balance can be written: $kR_{max} = M\omega^2 R_{max}$, which yields $\Omega = (M\omega^2/k) = $ constant.

Two-lobed shapes need to be sketched separately, to define the different parameters (figure 7). We have here two quasi-spherical lobes of radius h connected by a cylinder of radius b. Because of centrifugal force, the pressure must be larger in the lobes than in the cylinder, which yields $b > h/2$. If $b \sim h$ (thick peanut), the pressure gradient ∇P is of order $\gamma/(hR_{max})$, and the volume conservation is $R_{max}h^2 \sim R_0^3$. Balancing ∇P with the centrifugal force gives

$$R_{max} \sim R_0 \, \Omega_s^{-4/3}. \tag{14}$$

If $b \ll h$ (stretched peanut), the volume is mainly in the lobes ($h^3 \sim R_0^3$), and we thus have

$$R_{max} \sim R_0 \, \Omega_s^{-1/2}. \tag{15}$$

All these different scalings are compared in figure 8 with the numerical data. In each case, the fit can only be done for a limited range of rotation number Ω_s, but equations (9) to (15) portray fairly well the different regimes found numerically, which provides a physical picture of the force balance for each shape. The numerical coefficients deduced from the fits are all found to be of the order of unity (between 0.6 and 1.2). All the scaling formulae thus allow us to calculate very simply orders of magnitude of the different sizes, together with their non-trivial relationship with the rotation speed.
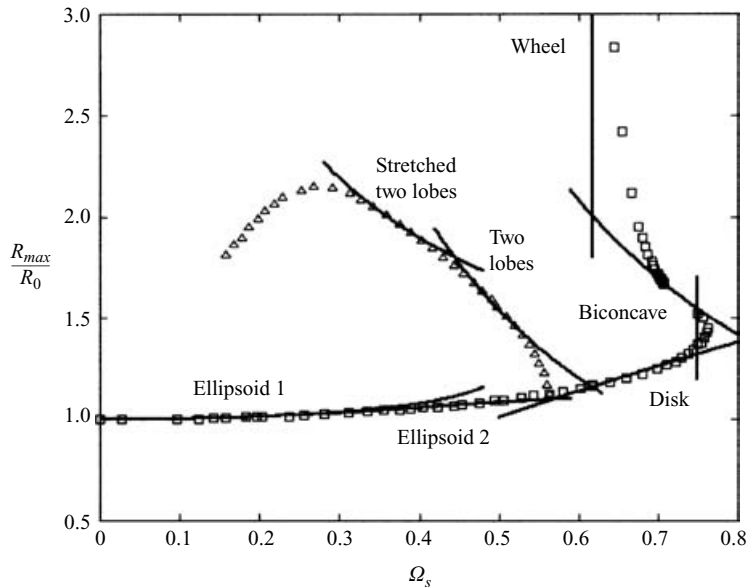
FIGURE 8. Numerical shapes (symbols) and scaling laws (equations (9) to (15), drawn as solid lines) for rotating liquid drops.

3. Experimental shapes of rotating liquid marbles

3.1. *Experimental method*

Our experiment consisted of placing a viscous liquid marble of radius R_0 either on an inclined plate or in a rotating drum. The plate is a polished metallic bar, and the drum made with nylon; its radius is 6 cm, i.e. more than twenty times the size of the drops. The drop motion was filmed using a high-speed camera (1000 frames per second). On the tilted plane, the position x of the drop was measured as a function of time after having rolled down a distance larger than 1 m, from which we could deduce the marble velocity ($V = \mathrm{d}x/\mathrm{d}t$). The maximum size of the drops was extracted from the movies.

For the two-lobed shapes, we measured, as a function of time, the angle θ between the axis passing through the lobes and a fixed direction. A straight line was obtained (figure 9), giving the angular speed ω. For axisymmetric shapes, we added tracers on the drop surface (such as pieces of iron filings with the lycopodium powder used for the coating) and followed the position of these tracers as a function of time, as can be seen in figure 10 where the tracers appear dark.

The trajectory of the tracers was found to be circular in each case, and the curvilinear coordinate s for each tracer (i.e. at a given distance from the axis of rotation) to vary linearly with time. For each experiment, we averaged on four tracers, placed at various distances r from the shape centre. The angular speed could finally be deduced from these measurements, with a scatter of about 10%. We also determined the radius R of each stationary shape.

3.2. *Results*

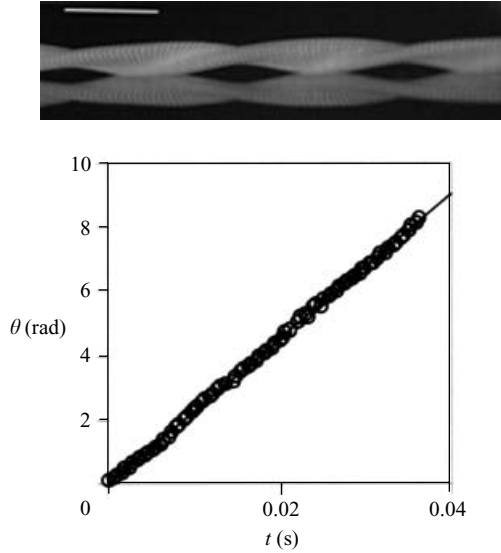We define the speed of rotation V_R as

$$V_R = R\omega. \tag{16}$$

FIGURE 9. Motion (from left to right) of a two-lobed shape (volume 5μl) running down a plane inclined by 37°. (We also see the reflection of the moving drop in the substrate.) The bar represents 1 cm and there is 0.44 ms between each shot. We also display the angular position θ of the shape as a function of time. The slope is 225 rad s^{-1}.
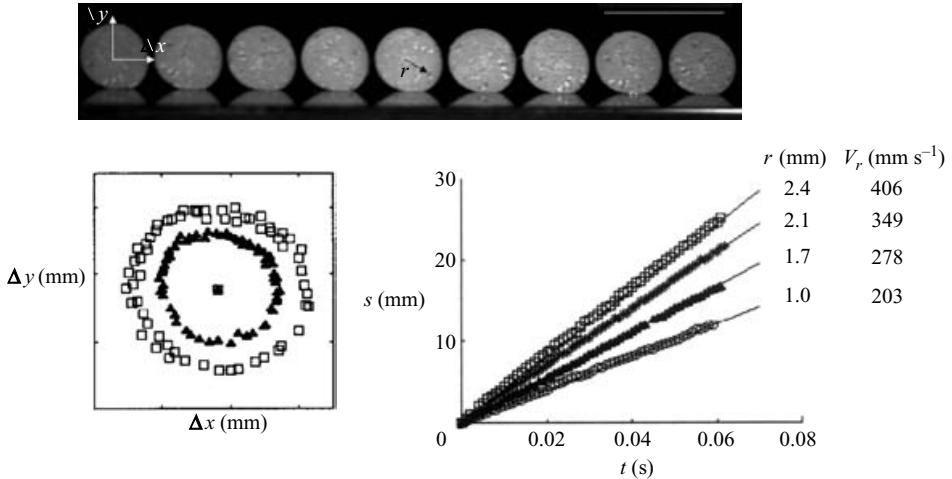

FIGURE 10. Measurement of the angular speed of an axisymmetric drop ($R_0 = 1.9$ mm) running down an incline (27°). 8 ms separate each snapshot, and the bar represents 1 cm. We follow the position of different tracers (placed at a distance r from the centre) as a function of time. Each trajectory is observed to be circular. The time evolution of the curvilinear coordinate s gives the angular speed $\omega = V_r/r$, which is here about 180 ± 20 rad s^{-1}.

Figure 11 shows how the (translational) drop speed V is related to V_R, all quantities in (16) being measured independently, as shown above.

At a low speed, the drops are quasi-spherical, and we simply find $V = V_R$. The drops rotate without sliding. But at a high speed (for the very deformed shapes), the situation is quite different: the rotation speed V_R reaches a plateau value, which is independent of the translational velocity V. As V increases (by one decade, between
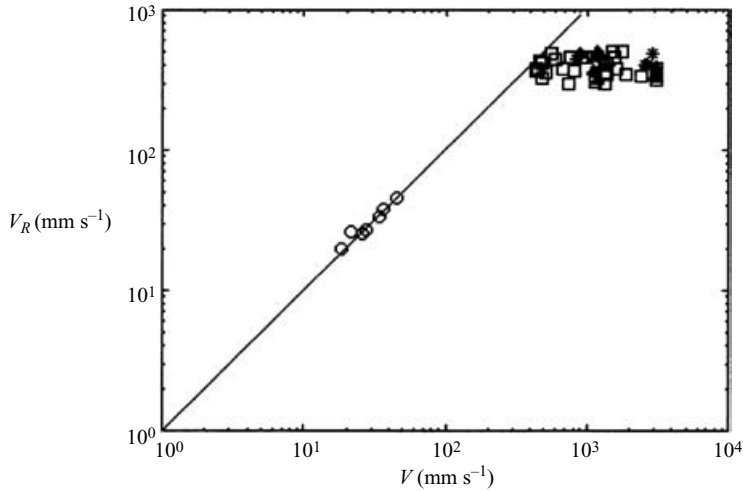
FIGURE 11. Speed of rotation of a liquid marble (as defined by equation (16)), as a function of the drop translational velocity. The circles correspond to quasi-static shapes (spheres), the squares to disks and biconcave shapes, the stars to wheels and the black triangles to two-lobed shapes. The solid line represents the equation $V_R = V$.
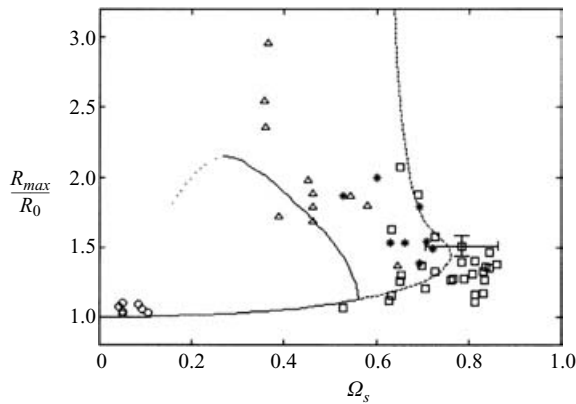

FIGURE 12. Maximum size of a rotating liquid marble (normalized by its initial size R_0), as a function of the rotation number Ω_s (equation (1)). The lines represent the numerical calculations (solid lines for the stable shapes). The circles correspond to quasi-spheres, the squares to disks or biconcave shapes, the stars to wheels and the triangles to two-lobed shapes. We indicated the typical error bars for one measurement.

0.4 and $3\,\mathrm{m\,s^{-1}}$), V_R is observed to remain nearly constant, between 0.3 and $0.5\,\mathrm{m\,s^{-1}}$. At a high speed, the drops are thus rotating and sliding, whatever their shape (disk, biconcave, wheel or two-lobed).

These experiments, finally, allow us to evaluate the speed of rotation (since we found here that it generally cannot be simply deduced from the translational speed, assuming a rotation without sliding), and thus to calculate the rotation number Ω_s for each experiment – a condition for establishing a phase diagram. In figure 12, we compare the experimental data with the numerical calculations, by plotting the maximum size R_{max} (normalized by the size at rest R_0) as a function of Ω_s, specifying
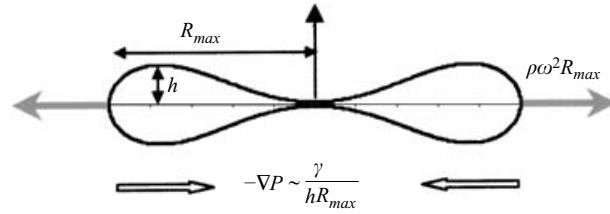
FIGURE 13. Biconcave rotating drop (cut view) obtained numerically ($\Omega_s = 0.71$), and forces
acting on it.

for each data point the nature of the observed shape (ellipsoid, two-lobed, disk or
biconcave, and wheel).

The data, obtained for various tilting angles of the incline ($10°$ to $50°$) and different
viscosities (0.3 to $1.1\,\mathrm{Pa\,s}$), are scattered, yet qualitatively agree with the numerical
predictions for all the shapes. In particular, the axisymmetric drops are systematically
found to correspond to higher values of the rotation number than the two-lobed
ones. The absolute values of the predicted rotation number for a given shape are also
in quite good agreement with the observations. We indicate in one case typical error
bars. They primarily come from an error in the determination of Ω_s, a tedious task
which must be performed for each moving shape, because of the possible existence
of a slip below the rotating drop, as stressed in figure 11. A smaller error originates
from the measurement of R_{max}, which can vary slightly with time, in particular for
the most elongated shapes. Note also that we never observed very large wheels, in
spite of the presence in the phase diagram of a vertical asymptote (which suggests
that wheels of different shapes should coexist for a given Ω_s). This may be due to the
forces acting on a large wheel, such as the weight, which tends to pinch it, and thus
to induce an instability towards a two-lobe shape, as we see in the next section.

4. Transformations

We have shown in figures 2, 9 and 12 that moving liquid marbles naturally form
two-lobed shapes. However, they can be axisymmetric as well (figures 2, 10 and
12), although these states should be unstable (dotted line in figures 1 and 12), as
shown by Chandrasekhar (1965) and Brown & Scriven (1980a). We thus wondered
if it were possible to induce transitions between the different shapes, which would
give a hint of their relative stability. We report in this section two examples of such
transformations. First, we study the transformation between an axisymmetric shape
(wheel or biconcave) and a two-lobed one. Then, we focus on the possible evolution
of a 'peanut'.

4.1. The doughnut/peanut transition

As emphasized above, most of the drop shapes obtained on an incline are toroidal
or biconcave, and thus presumably unstable if compared with two-lobed ones.
We first discuss here the physical origin of this instability, considering asymmetric
perturbations. Then we check experimentally the stability of the axisymmetric shapes
and discuss the results.

4.1.1. Stability analysis

We consider a shape predicted to be unstable by Brown & Scriven, and take as
an example a biconcave (or toroidal) drop (figure 13). As seen above (equation (12)),
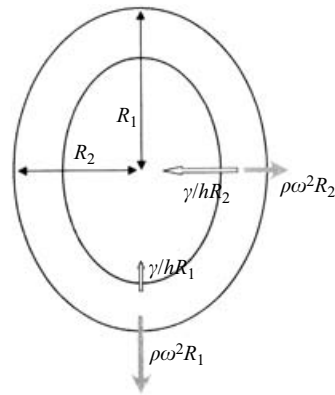
FIGURE 14. Sketch of an asymmetrically perturbed toroidal drop, and forces acting on it.

FIGURE 15. Toroidal glycerol marble leaving its substrate and falling freely in air. We observe a spontaneous (and irreversible) transformation towards a two-lobed shape. 4 ms separates each image, the drop has an initial radius $R_0 = 2.1$ mm and the bar represents 1 cm.

this shape results from a balance between the centrifugal force and surface tension, that is, $\rho\omega^2 R_{max}$ and $\gamma/(hR_{max})$, per unit volume. We now consider an asymmetric perturbation of this shape, as sketched in figure 14 (where we represent a side view of the drop, instead of a cut, as in figure 13). The perturbation makes the drop slightly elliptic, and we denote the respective axes as R_1 and R_2 ($R_2 < R_{max} < R_1$). Compared with a circular wheel, the capillary restoring force is larger on the small axis, and smaller on the large one. It is the opposite for the centrifugal force (grey arrows in figure 14), and the wheel thus tends to pinch and to transform into a two-lobed shape. Isolated toroidal or biconcave drops should indeed be unstable, as predicted numerically by Brown & Scriven.

4.1.2. *Experimental observations*

The main difference between our experiment and the previous ones (Wang *et al.* 1986, 1994; Lee *et al.* 1998) or the ideal situation considered by Brown & Scriven (1980*a*) lies in the presence of a solid below the drop, on which it can roll. In order to check how the substrate influences the stability of the toroidal and biconcave shapes, we performed an experiment where the substrate ended at some point (Elkins-Tanton *et al.* 2003).

The pictures displayed in figure 15 are obtained by allowing a glycerol marble ($R_0 = 2.1$ mm) coated with lycopodium to run down a plate tilted by $40°$ (the camera is tilted by the same angle). It has a toroidal shape at the end of the substrate, and then jumps into air. Immediately after having left the substrate, the marble begins to transform into a two-lobed shape. This transformation occurs via a pinching, as
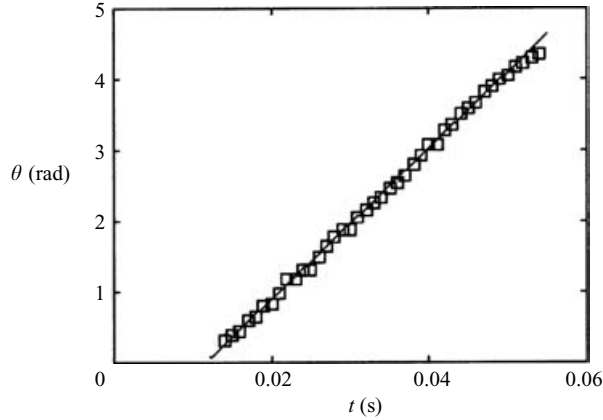
FIGURE 16. Angular position of the main axis of the drop as a function of time. The straight line indicates a slope of $107\,\mathrm{rad\,s^{-1}}$. The drop leaves the inclined plane at $t_0 = 0.01\,\mathrm{s}$.
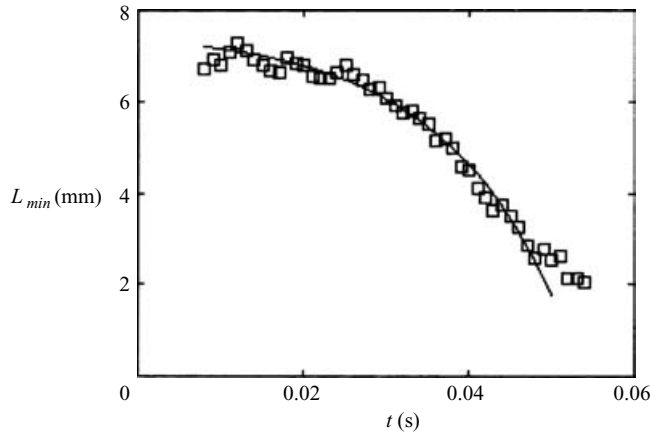

FIGURE 17. Size L_{min} of the small axis of the drop as a function of time. The line represents an exponential decrease of characteristic time $\tau = 15\,\mathrm{ms}$. The drop leaves the plate at $t_0 = 0.01\,\mathrm{s}$.

assumed in figure 14, and takes a few tens of milliseconds (this short time scale indicates that inertia dominates viscosity in this process). As predicted by Brown & Scriven, an isolated toroidal drop is less stable than a peanut shape, which shows that the observed axisymmetric shapes were stabilized by the presence of a solid substrate.

We can follow the evolution of the drop during its transformation. First, the position of the centre of inertia is found to be simply given by the law of free fall in air (parabolic trajectory in figure 15). Secondly, we can measure the angular position of the main axis of the drop as a function of time, as shown in figure 16. The transformation occurs at a constant angular speed, here $\omega = 107\,\mathrm{rad\,s^{-1}}$. In figure 17, we show the size $L_{min} = 2R_2$ of the small axis of the drop as a function of time, to monitor the dynamics of the pinching. The size of the small axis is observed to decrease with time, and this variation turns out to be nicely fitted at short time by an exponential law. It yields a characteristic time τ for pinching, which is observed in this example to be about 15 ms. This τ can be compared with the time needed by the drop to make a complete turn, which is about 59 ms here. Both these times are thus of the same order, which emphasizes that axisymmetric drops are weakly stable.
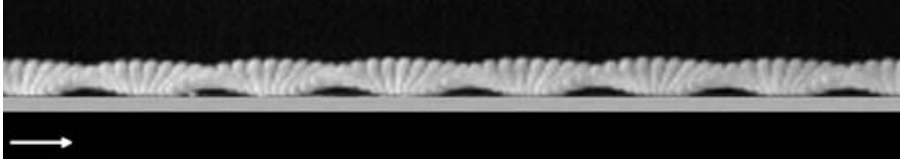
FIGURE 18. Two-lobed marble ($\eta = 200\,\text{mPa s}$, $R_0 = 1.33$ mm) running down an incline (tilting angle of $36°$). The motion is stable over more than 15 cm (the size of the picture).

4.1.3. *Discussion*

As reported above, both axisymmetric and two-lobed shapes are observed for liquid marbles running down an incline. This means that two-lobed drops can appear spontaneously. Most often, this occurs via a deformation of a toroidal or biconcave drop into a slightly elliptic shape (which could be due to gravity), which eventually makes the drop spontaneously jump, and then transform into a peanut shape. It is important to note that this transformation is irreversible: once a peanut shape is achieved, it is observed to be stable and we never observed experimentally any reverse transformation (neither spontaneous nor forced) from a two-lobed shape to an axisymmetric one. In addition, smaller droplets were found to have a tendency to make two-lobed shapes directly.

It was observed by Ohsaka & Trinh (2000) that three-lobed shapes can be obtained by way of forbidden two-lobed perturbations. Similarly we can consider that the growth of the perturbation leading to two-lobed shapes is not favoured in our experiment by the presence of a solid substrate. It was emphasized above that the drop must leave the solid to transform. The presence of a (dynamic) film of air below the moving drop (generating a Bernoulli lower pressure below the drop) might induce an efficient sticking mechanism for the drop. The drop weight should also contribute to prevent take-off (and it was indeed observed that smaller drops, i.e. lighter ones, spontaneously transform much more easily into peanuts). But a complete treatment of the stabilization mechanism is left as a subject for future consideration.

We can briefly discuss the dynamics of pinching. As suggested in figure 14, the driving force is a gradient of Laplace pressure $\gamma/(hR_2)$. At the beginning of the process, we can write $R_2 = R_{max} - \varepsilon$, which allows us to expand the capillary force. Balancing the Laplace force with inertia $\rho\,\mathrm{d}^2\varepsilon/\mathrm{d}t^2$, we obtain a linear equation, with a solution of the form $L_{min} = 2R_2 = 2R_{max} - a\exp(t/\tau)$, an exponential variation of the characteristic time $\tau = \sqrt{\rho h R_{max}^2/\gamma}$. This dependence is in agreement with the observations in figure 17, from which we deduce a time τ of about 15 ms, in agreement with the value calculated from the expression above.

Later, the equations can no longer be linearized, and the force balance is $\rho\,\mathrm{d}^2 R_2/\mathrm{d}t^2 = \gamma/(hR_2)$. This equation has no analytical solution. Treating it at a scaling level ($\rho R_2/t^2 \sim \gamma/(hR_2)$) suggests a solution close to linear in time. (Numerical solutions confirm that behaviour.) This result is in fair agreement with the data displayed in figure 17, where the late steps of pinching ($t > 0.04$ s) are (close to) linear in time.

4.2. *Evolution of free two-lobed drops*

4.2.1. *Experimental observations*

Once a two-lobed shape is achieved on a plane, it is remarkably stable, as shown in figure 18 where a stable peanut form is observed over a span exceeding 15 cm. On the other hand, a free peanut evolves and eventually separates into two spheres
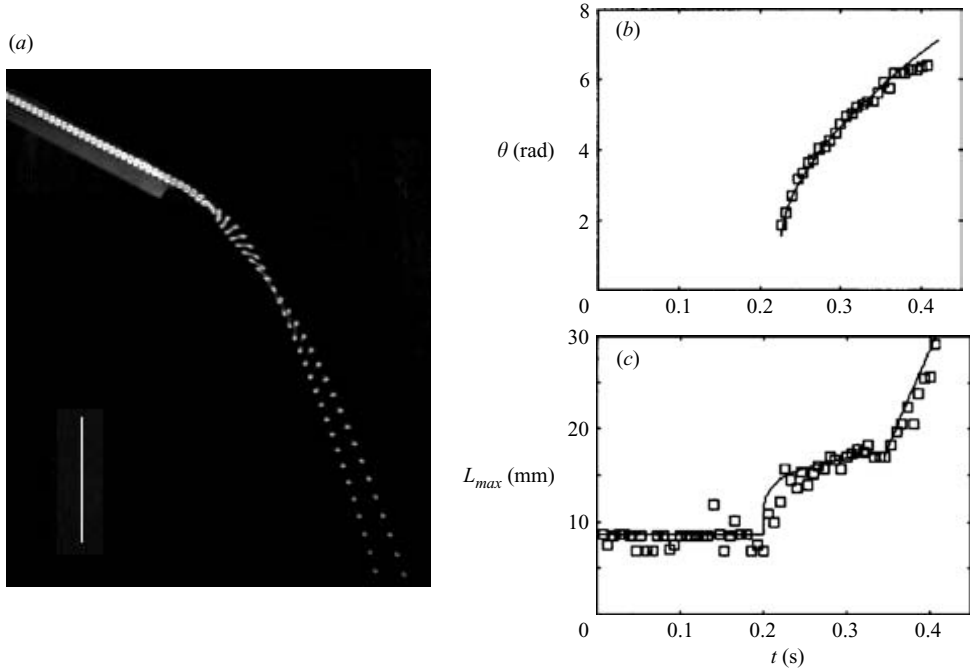
FIGURE 19. (*a*) Glycerol marble ($R_0 = 2.12$ mm) falling from an incline (tilted by $27°$). The white line is 10 cm and 6.6 ms separates each image. Once in air, the drop loses its axisymmetric shape, and eventually separates into two spheres. (*b*) Angular position θ of the marble corresponding to the experiment displayed in (*a*). The curved line, $\theta = 15 \, (t - 0.23)^{0.6}$, corresponds to equation (20). (*c*) Maximum size L_{max} of a the marble corresponding to the experiment displayed in (*a*). The two solid lines, corresponding to $\theta = 15 \, (t - 0.23)^{0.2}$ and $\theta = 210 \, (t - 0.35)$, respectively, originate from equations (19) and (21).

(Figure 19*a*). We can follow in this experiment the angular position of the drop as a function of time (figure 19*b*), together with the evolution of its maximal size $L_{max} = 2R_1$ (figure 19*c*). For $t < 0.23$ s, the drop still is toroidal, which makes it difficult (in the absence of tracers) to follow the angular motion. We do not report any data in this regime, which was described in figure 10. As the drop leaves its substrate ($t > 0.23$ s), it quickly transforms into a peanut shape (the time scale of the transformation was found to be around 20 ms, thus much shorter than the time scale of the experiment in figure 19. Then, θ increases (the peanut rotates), and the angular speed is observed to decrease in this regime, as it can be expected for an isolated elongating drop with a constant angular momentum.

The time evolution of the drop size can be decomposed in three parts. First, till $t = 0.2$ s, the drop is on the incline: it is axisymmetric, with a constant size (stationary torus). Then, the drop leaves the plate and its size increases in a nonlinear manner (elongation of the peanut). Finally, at $t = 0.35$ s, the drop breaks into two parts, and L_{max} then denotes the distance between them. This distance is observed to increase linearly with time.

4.2.2. *Scaling laws*

We assume that a two-lobed shape can be described as two spheres (which include all the drop mass, and whose radius remains of the order of R_0), connected by a cylinder of constant negligible volume and diameter b ($b \ll R_0$). As time goes on,
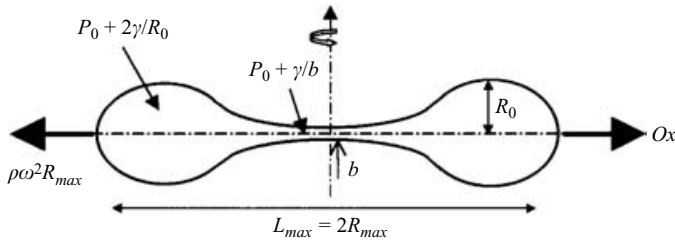
FIGURE 20. Sketch of an elongating two-lobed drop.

this cylinder elongates and becomes thinner (figure 20). The drop is isolated, with a constant angular momentum. With this hypothesis, the moment of inertia $J \sim m L_{max}^2$ of the drop depends only on the maximum size and mass of the drop. Denoting L_0 and ω_0 as the maximum size and angular speed of the drop just after the transformation from an axisymmetric to a two-lobed shape, we can express the conservation of angular momentum as

$$L_{max}^2 \omega \sim L_0^2 \omega_0. \tag{17}$$

During breakup, centrifugal forces dominate surface tension, and thus the destabilizing force acting on the drop can be written

$$f \sim m\,\omega^2\,L_{max}. \tag{18}$$

Two forces oppose the drop elongation, namely inertia and viscous friction. On the one hand, inertia can be written $f \sim m\ddot{L}_{max}$. On the other hand, the viscous force arises from the friction of liquid inside the cylinder, which behaves as a solid pipe, because of the presence of the grains. It is thus given by the Poiseuille formula: $f \sim \eta L_{max} \dot{L}_{max}$. We deduce that inertia can be neglected if the characteristic time τ_L for the evolution of the shape satisfies

$$\tau_L \gg \frac{\rho R_0^3}{\eta L_{max}}.$$

For a drop of size 1 millimetre, the second term of this inequality is less than 1 ms. The evolution of the shape takes place in typically 100 ms, so that this inequality is fully fulfilled. Balancing the centrifugal force with the viscous one, and assuming a constant volume for the cylinder ($L_{max} b^2 \sim L_0 b_0^2$, where b_0 is the arm radius when the drop size is L_0), yields as a scaling law for the dynamics of elongation:

$$L_{max} \sim \left(\frac{\rho R_0^3 L_0^4 \omega_0^2}{\eta} \right)^{1/5} t^{1/5}. \tag{19}$$

Using (17), we deduce the angular evolution:

$$\theta \sim \left(\frac{\eta\, L_0\, \omega_0^{1/2}}{\rho\, R_0^3} \right)^{2/5} t^{3/5}. \tag{20}$$

Both laws are observed to describe the data quite well, in figure 19. In addition, the coefficients deduced from the fits are respectively 15 and 1.3×10^{-2}, close to the coefficients which can be calculated in equations (19) and (20) (from which we find 30 and 2×10^{-2}).

Once the two lobes separate, the motion of each sphere is a free fall and the two parts continue to move away from each other following the law

$$L_{max} - L_{rup} \sim L_{rup}\omega_{rup}(t - t_{rup}),\tag{21}$$

where L_{rup} and ω_{rup} are respectively the size and angular speed of the two-lobe shape just prior to the rupture, which occurs at $t = t_{rup}$. A linear law describes the data (figure 19c), with a characteristic speed $0.21\,\mathrm{m\,s^{-1}}$, close to the value which can be deduced from the experiment $L_{rup}\omega_{rup} = 0.14\,\mathrm{m\,s^{-1}}$.

5. Conclusion

We have described in this paper the shape of moving liquid marbles. These are non-wetting drops which rotate as they move. Because of the fast motion due to the absence of a contact line, the shapes are often found to differ dramatically from the static case, for which the marbles are quasi-spherical. These shapes show the rolling motion of the drops: disks, wheels and peanut shapes were observed, and interpreted as resulting from a balance between centrifugal and capillary forces. The dependence of the maximum drop size R_{max} on the rotation number Ω_s was justified in the various regimes by way of simple scaling arguments. It was also found that in the regime of large deformation, the motion is a superimposition of rolling and slippage, forcing us to study separately both dynamics – in order to compare the actual shapes with the numerical predictions.

We focused particularly on the toroidal shape, which was shown to be a solution of the equations of motion, allowing us to include it in the phase diagram of revolving drops established by Brown & Scriven. But as predicted by Chandrasekhar and Brown & Scriven, we also found that this shape was metastable. If forced to leave the substrate, it spontaneously (and irreversibly) transforms into a peanut shape. We characterized the dynamics of the transformation, and also the elongation (and possible breakage) of the two-lobed shape resulting from this instability. The mechanism stabilizing the tori on inclines remains to be elucidated, but as a practical consequence, these drops run down without leaving a trail – an unusual and interesting property if the aim is to move (quickly) a liquid body on a solid without any leakage.

REFERENCES

AUSSILLOUS, P. & QUÉRÉ, D. 2001 Liquid marbles. *Nature* **411**, 924–927.

BOHR, N. & WHEELER, J. A. 1939 The mechanism of nuclear fission. *Phys. Rev.* **55,** 426–450.

BOUASSE, H. 1924 *Capillarité et Phénomènes Superficiels*. Delagrave, Paris.

BROWN, R. A. & SCRIVEN, L. E. 1980a The shape and stability of rotating liquid drops. *Proc. R. Soc. Lond.* A **371**, 331–357.

BROWN, R. A. & SCRIVEN, L. E. 1980b New class of asymmetric shapes of rotating liquid. *Phys. Rev. Lett.* **45**, 180–183.

CHANDRASEKHAR, S. 1965 The stability of a rotating liquid drop. *Proc. R. Soc. Lond.* A **286**, 1–26.

COHEN, S., PLASIL, F. & SWIATECKI, W. J. 1974 Equilibrium configurations of rotating charged or gravitating liquid masses with surface tension. II. *Annals Phys.* **82**, 557–596.

ELKINS-TANTON, L. T., AUSSILLOUS, P., BICO, J., QUÉRÉ, D. & BUSH J. W. M. 2003 A laboratory model of splash-form tektites. *Meteoritics Planet. Sci.* **38**, 1331–1340.

LAPLACE, P. S. 1843–1847 *Œuvres Complètes*. Imprimerie Royale, Paris.

LEE, C. P., ANILKUMAR, A. V., HMELO, A. B. & WANG, T. G. 1998 Equilibrium of liquid drops under the effects of rotation and acoustic flattening: results from USML-2 experiments in Space. *J. Fluid Mech.* **354**, 43–67.

MAHADEVAN, L. & POMEAU, Y. 1999 Rolling droplets. *Phys. Fluids* **11**, 2449–2453.

OHSAKA, K. & TRINH, E. H. 2000 Three-lobed shape bifurcation of rotating liquid drops. *Phys. Rev. Lett.* **84**, 1700–1703.

PLATEAU, J. A. F. 1843–1869 Recherches expérimentales et théoriques sur les figures d'équilibre d'une masse liquide sans pesanteur. *Mém. Acad. R. Sci. Lett. Belg*. Vol. 16–37.

POINCARÉ, H. 1885 Sur l'équilibre d'une masse fluide animée d'un mouvement de rotation. *Acta Mathematica* **7**, 259–380.

RAYLEIGH, LORD 1914 The equilibrium of revolving liquid under capillary force. *Phil. Mag.* **28**, 161–170.

ROSS, D. K. 1968 The shape and energy of a revolving liquid mass held together by surface tension. *Aust. J. Phys.* **21**, 823–835.

WANG, T. G., ANILKUMAR, A. V., LEE, C. P. & LIN, K. C. 1994 Bifurcation of rotating liquid drops: results from USML-1 experiments in Space. *J. Fluid Mech* **276**, 389–403.

WANG, T. G., TRINH, E. H., CROONQUIST, A. P. & ELLEMANT, D. D. 1986 Shapes of rotating free drops: spacelab experimental results. *Phys. Rev. Lett.* **56**, 452–455.